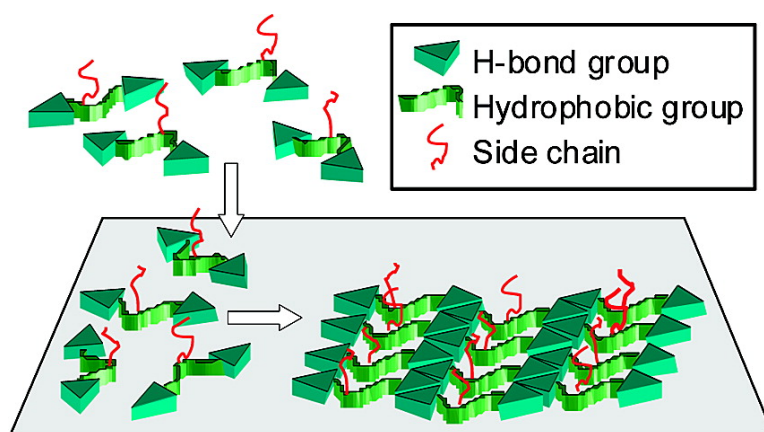Article

Molecular Engineering of Supramolecular Scaffold Coatings that Can Reduce Static Platelet Adhesion

Aryavarta M. S. Kumar, Sona Sivakova, Justin D. Fox,
Jennifer E. Green, Roger E. Marchant, and Stuart J. Rowan

More About This Article

Additional resources and features associated with this article are available within the HTML version:

- Supporting Information
- Links to the 1 articles that cite this article, as of the time of this article download
- Access to high resolution figures
- Links to articles and content related to this article
- Copyright permission to reproduce figures and/or text from this article

View the Full Text HTML

Molecular Engineering of Supramolecular Scaffold Coatings that Can Reduce Static Platelet Adhesion

Aryavarta M. S. Kumar,[†] Sona Sivakova,[‡] Justin D. Fox,[‡] Jennifer E. Green,[†] Roger E. Marchant,[*,†,‡] and Stuart J. Rowan[*,‡,†,§]

Center for Cardiovascular Biomaterials, Department of Biomedical Engineering and Department of Macromolecular Science and Engineering, and Department of Chemistry, Case Western Reserve University, Cleveland Ohio 44106

Received October 2, 2007; E-mail: stuart.rowan@case.edu; roger.marchant@case.edu

Abstract: Novel supramolecular coatings that make use of low-molecular weight ditopic monomers with guanine end groups are studied using fluid tapping AFM. These molecules assemble on highly oriented pyrolytic graphite (HOPG) from aqueous solutions to form nanosized banding structures whose sizes can be systematically tuned at the nanoscale by tailoring the molecular structure of the monomers. The nature of the self-assembly in these systems has been studied through a combination of the self-assembly of structural derivatives and molecular modeling. Furthermore, we introduce the concept of using these molecular assemblies as scaffolds to organize functional groups on the surface. As a first demonstration of this concept, scaffold monomers that contain a monomethyl triethyleneglycol branch were used to organize these "functional" units on a HOPG surface. These supramolecular grafted assemblies have been shown to be stable at biologically relevant temperatures and even have the ability to significantly reduce static platelet adhesion.

Introduction

Supramolecular chemistry at the interface plays a defining role in the "bottom-up" approach to nanoarchitectures which have a myriad of potential technological applications in areas such as nanoelectronics, biological coatings, and catalytic processes.[1,2] In designing new solid−liquid interfacial (surface) assemblies, both surface−adsorbate and adsorbate−adsorbate interactions need to be taken into account.[3] For instance, designing the correct interactions between a molecule and a surface can be critical in creating ordered surface assemblies. Thus, designing the appropriate surface−adsorbate interactions can be a powerful tool in controlling the nature of the molecular surface assembly. For example, long alkyl chains are known to form highly ordered (epitaxial) surface assemblies commensurate with the ordered lattice of graphite.[4,5] In addition, tailoring the supramolecular interactions (such as hydrogen bonding, alkyl−alkyl interactions, etc.) between the molecules (adsorbates) can also be employed to tune the nature of the resulting stable, ordered surface assemblies. By manipulating both surface−adsorbate and adsorbate−adsorbate interactions, a number of groups have studied the potential of physisorbed compounds to facilitate molecular assembly on ordered surfaces.[2,6,7]

One class of supramolecular motifs that has received attention in the area of self-assembly over the years is the nucleobases.[8,9] Of particular interest are guanine derivatives, which have the

---

[†] Center for Cardiovascular Biomaterials, Department of Biomedical Engineering.
[‡] Department of Macromolecular Science and Engineering.
[§] Department of Chemistry.

(1) (a) Ryu, D. Y.; Shin, K.; Drockenmuller, E.; Hawker, C. J.; Russell, T. P. *Science* **2005**, *308*, 236−239. (b) Michl, J.; Magnera, T. F. *Proc. Natl. Acad. Sci. U.S.A.* **2002**, *99*, 4788−4792. (c) Schönherr, H.; Paraschiv, V.; Zapotoczny, S.; Crego-Calama, M.; Timmerman, P.; Frank, C. W.; Vancso, G. J.; Reinhoudt, D. N. *Proc. Natl. Acad. Sci. U.S.A.* **2002**, *99*, 5024−5027. (d) Russell, T. P. *Science* **2002**, *297*, 964−967. (e) Leclère, P.; Surin, M.; Jonkheijm, P.; Henze, O.; Schenning, A. P. H. J.; Biscarini, F.; Grimsdale, A. C.; Feast, W. J.; Meijer, E. W.; Müllen, K.; Brédas, J.-L.; Lazzaroni, R. *Eur. Polym. J.* **2004**, *40*, 885−892.

(2) (a) Palermo, V.; Liscio, A.; Gentilini, D.; Nolde, F.; Müllen, K.; Samorì, P. *Small* **2007**, *3*, 161−167. (b) Puigmartí-Luis, J.; Minoia, A.; Uji-i, H.; Rovira, C.; Cornil, J.; De Feyter, S.; Lazzaroni, R.; Amabilino, D. B. *J. Am. Chem. Soc.* **2006**, *128*, 12602−12603. (c) Xu, H.; Norsten, T. B.; Uzun, O.; Jeoung, E.; Rotello, V. M., *Chem. Commun.* **2005**, 5157−5159.

(3) (a) Barth, J. V.; Costantini, G.; Kern, K. *Nature* **2005**, *437*, 671−679. (b) Badin, M. G.; Bashir, A.; Krakert, S.; Strunskus, T.; Terfort, A.; Wöll, C. *Angew. Chem., Int. Ed.* **2007**, *46*, 3762−3764. (c) Li, S.-S.; Yan, H.-J.; Wan, L.-J.; Yang, H.-B.; Northrop, B. H.; Stang, P. J. *J. Am. Chem. Soc.* **2007**, *129*, 9268−9269.

(4) (a) Leunissen, M. E.; Graswinckel, W. S.; van Enckevort, W. J. P.; Vlieg, E. *Cryst. Growth Des.* **2003**, *4*, 361−367. (b) Stepanow, S.; Lin, N.; Barth, J. V.; Kern, K. *Chem. Commun.* **2006**, 2153−2155.

(5) Groszek, A. J. *Proc. R. Soc. London, A* **1970**, *314*, 473−498.

(6) (a) Barth, J. V.; Weckesser, J.; Cai, C.; Günter, P.; Bürgi, L.; Jeandupeux, O.; Kern, K. *Angew. Chem., Int. Ed.* **2000**, *39*, 1230−1234. (b) Tao, F.; Bernasek, S. L. *J. Am. Chem. Soc.* **2005**, *127*, 12750−12751. (c) Griessl, S. J. H.; Lackinger, M.; Jamitzky, F.; Markert, T.; Hietschold, M.; Heckl, W. M. *Langmuir* **2004**, *20*, 9403−9407. (d) Kim, K.; Matzger, A. J. *J. Am. Chem. Soc.* **2002**, *124*, 8772−8773. (e) Qian, P.; Nanjo, H.; Yokoyama, T.; Suzuki, T. M. *Chem. Commun.* **1999**, 1197−1198. (f) Nath, K. G.; Ivasenko, O.; Miwa, J. A.; Dang, H.; Wuest, J. D.; Nanci, A.; Perepichka, S. F.; Rosei, F. *J. Am. Chem. Soc.* **2006**, *128*, 4212−4213. (g) Hipps, K. W.; Scudiero, L.; Barlow, D. E.; Cooke, M. P. Jr. *J. Am. Chem. Soc.* **2002**, *124*, 2126−2127. (h) Theobald, J. A.; Oxtoby, N. S.; Phillips, M. A.; Champness, N. R.; Beton, P. H. *Nature* **2003**, *424*, 1029−1031. (i) Canas-Ventura, M. E.; Xiao, W.; Wasserfallen, D.; Müllen, K.; Brune, H.; Barth, J. V.; Fasel, R. *Angew. Chem., Int. Ed.* **2007**, *46*, 1814−1818. (j) Baker, R. T.; Mougous, J. D.; Brackley, A.; Patrick, D. L. *Langmuir* **1999**, *15*, 4884−4891. (k) Stevens, F.; Beebe, T. P., Jr. *Langmuir* **1999**, *15*, 6884−6889. (l) Hecht, S. *Angew. Chem., Int. Ed.* **2003**, *42*, 24−26. (m) Yablon, D. G.; Ertas, D.; Fang, H.; Flynn, G. W. *Isr. J. Chem.* **2003**, *43*, 383−392. (n) Cox, J. K.; Eisenberg, A.; Lennox, R. B. *Curr. Opin. Colloid Interface Sci.* **1999**, *4*, 52−59. (o) Gong, J.-R.; Yan, H.-J.; Yuan, Q.-H.; Xu, L.-P.; Bo, Z.-S.; Wan, L.-J. *J. Am. Chem. Soc.* **2006**, *128*, 12384−12385.
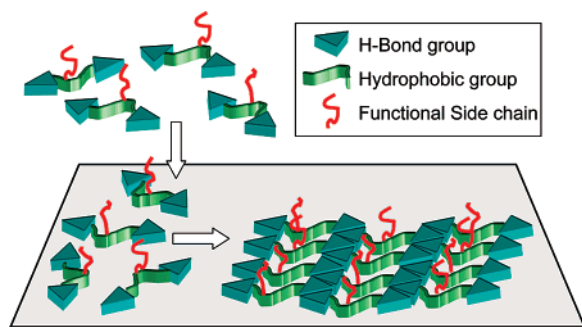
Figure 1. Concept of organized functional groups arranged through surface supramolecular polymerization. Monomers are initially in solution followed by adsorption and assembly to form linear band structures that present side groups in an ordered array on a hydrophobic surface.

ability to interact with themselves or with complementary motifs through the use of Watson−Crick binding and/or Hoogsteen binding. For example, when guanine and its derivatives are adsorbed on a graphite surface, the resulting aggregates can form ordered tapes or monolayers that can make use of guanine−guanine interactions,[10,11] in addition to surface−adsorbate interactions.

In recent years, a number of groups have investigated the potential of using oligonucleotides to self-assemble two-dimensional (2D) arrays and to use those as scaffolds to display a range of functionalities.[12] Recently, we initiated a program aimed at investigating the potential of assembling supramolecular polymers, derived from low-molecular weight nucleobase-endcapped monomers, on a surface[13] as a way to organize functional groups at the nanoscale (Figure 1) and as such act as molecular-scale surface scaffolds. In this manuscript, we report for the first time the realization of this concept. Using triethylene glycol monomethyl ether (TEG) groups attached to low-molecular weight monomers, these supramolecular scaffold-organized TEG surfaces exhibit reduced protein absorption and platelet adhesion. To further back up the nature and mechanism of this scaffold assembly a series of model compounds (without the TEG units) have been prepared and studied, allowing a better understanding of how these systems assemble on highly oriented pyrolytic graphite (HOPG).

The thromboresistance of biomaterial coatings is determined by its interaction with plasma proteins and platelets.[14] The most abundant plasma proteins, albumin, immunoglobulin, and fibrinogen, constitute the main adsorbed components on hydrophobic surfaces within microseconds of contact with blood.[15] Typically, over a period of time, an exchange process (Vroman effect) results in an increase in the proportion of thrombogenic proteins such as fibrinogen, kininogen, and factor XII on the surface.[16] The hydrophobic nature of the surface causes adsorbed proteins to denature, exposing peptide residues such as RGD that bind to specific platelet receptors such as GPIIb/IIIa (CD41/CD61). This sequence of events begins surface-induced thrombosis and causes many significant complications in implanted devices.[17] Healthy blood vessels provide a model to understand the prevention of surface-induced thrombosis. The glycocalyx on endothelial cells that line the lumen of blood vessels presents membrane proteins and carbohydrates that actively prevent thrombosis by creating a hydrated layer[18] at the surface which acts to reduce nonspecific protein adsorption, protein denaturation, and platelet adhesion. Thus, coatings that present groups that can mimic the hydrated layer most likely will have improved thromboresistance and blood biocompatibility.

A well-known strategy for creating protein resistant surfaces involves utilizing surface-bound polyethylene glycol (PEG) chains.[19−22] While a general theory of how PEG prevents protein adsorption is still being developed, it is currently thought that a hydrated PEG chain provides both osmotic (solvation of PEG chains) and entropic (conformational entropy of PEG chains) penalties that can be large enough to disfavor the hydrophobic interaction between proteins and the hydrophobic surface.[19,20c,23] Thus, in order for surface-bound PEG to work effectively to prevent protein adhesion it needs to be solvated with water molecules. Modeling studies suggest that when surface-bound PEG is hydrated it preferentially forms a random coil "helical" structure (*gauche−trans−gauche*).[18,23b,24] Thus, it has been proposed that PEG needs to be able to form these helical conformations in order to hydrate effectively and therefore prevent protein adhesion.[19,23b] For example, proteins are repelled when grafted PEG chains form helical conformations on Au

(7) (a) De Feyter, S.; De Schryver, F. C. *Chem. Soc. Rev.* **2003**, *32*, 139−150. (b) De Feyter, S.; Larsson, M.; Schuurmans, N.; Verkuijl, B.; Zoriniants, G.; Gesquière, A.; Abdel-Mottaleb, M. M.; Esch, J. v.; Feringa, B. L.; van Stam, J.; De Schryver, F. C. *Chem. Eur. J.* **2003**, *9*, 1198−1206. (c) Gesquière, A.; Jonkheijm, P.; Hoeben, F. J. M.; Schenning, A. P. H. J.; De Feyter, S.; De Schryver, F. C.; Meijer, E. W. *Nano Lett.* **2004**, *4*, 1175−1179. (d) Furukawa, S.; Tahara, K.; De Schryver, F. C.; Van der Auweraer, M.; Tobe, Y.; De Feyter, S. *Angew. Chem., Int. Ed.* **2007**, *46*, 2831−2834. (e) Mamdouh, W.; Uji-i, H.; Ladislaw, J. S.; Dulcey, A. E.; Percec, V.; De Schryver, F. C.; De Feyter, S. *J. Am. Chem. Soc.* **2006**, *128*, 317−325.
(8) (a) Seeman, N. C. *Trends Biotechnol.* **1999**, *17*, 437−443. (b) Li, Y.; Tseng, Y. D.; Kwon, S. Y.; D'Espaux, L.; Bunch, J. S.; McEuen, P. L.; Luo, D. *Nat. Mater.* **2004**, *3*, 38−42. (c) Xu, S.; Dong, M.; Rauls, E.; Otero, R.; Linderoth, T. R.; Besenbacher, F. *Nano Lett.* **2006**, *6*, 1434−1438.
(9) Sivakova, S.; Rowan, S. J. *Chem. Soc. Rev.* **2005**, *34*, 9−21.
(10) (a) Sowerby, S. J.; Edelwirth, M.; Heckl, W. M. *J. Phys. Chem. B* **1998**, *102*, 5914−5922. (b) Kelly, R. E. A.; Kantorovich, L. N. *J. Mater. Chem.* **2006**, *16*, 1894−1905.
(11) Gottarelli, G.; Masiero, S.; Mezzina, E.; Pieraccini, S.; Rabe, J. P. *Chem. Eur. J.* **2000**, *6*, 3242−3248.
(12) (a) Winfree, E.; Liu, F.; Wenzler, L. A.; Seeman, N. C. *Nature* **1998**, *394*, 539−544. (b) Park, S. H.; Yin, P.; Liu, Y.; Reif, J. H.; LaBean, T. H.; Yan, H. *Nano Lett.* **2005**, *5*, 729−733. (c) Zheng, J.; Constantinou, P. E.; Micheel, C.; Alivisatos, A. P.; Kiehl, R. A.; Seeman, N. C. *Nano Lett.* **2006**, *6*, 1502−1504. (d) Garibotti, A. V.; Knudsen, S. M.; Ellington, A. D.; Seeman, N. C. *Nano Lett.* **2006**, *6*, 1505−1507. (e) Ding, B.; Seeman, N. C. Science **2006**, *314*, 1583−1585. (f) Lin, C.; Liu, Y.; Yan, H. *Nano Lett.* **2007**, *7*, 507−512.
(13) Kumar, A. M. S.; Sivakova, S.; Marchant, R. E.; Rowan, S. J. *Small* **2007**, *3*, 783−787.
(14) (a) Horbett, T. A. *Cardiovasc. Pathol.* **1993**, *2*, 137s−148s. (b) Sharma, C. P. *J. Biomater. Appl.* **2001**, *15*, 359−381.
(15) Swalen, J. D.; Allara, D. L.; Andrade, J. D.; Chandross, E. A.; Garoff, S.; Israelachvili, J.; McCarthy, T. J.; Murray, R.; Pease, R. F.; Rabolt, J. F.; Wynne, K. J.; Yu, H. *Langmuir* **1987**, *3*, 932−950.
(16) (a) Vroman, L.; Adams, A. L. *Surf. Sci.* **1969**, *16*, 438−446. (b) Hudson, S. D.; Jung, H.-T.; Percec, V.; Cho, W.-D.; Johansson, G.; Ungar, G.; Balagurusamy, V. S. K. *Science* **1997**, *278*, 449−452.
(17) Ratner, B. D. *J. Biomed. Mater. Res.* **1993**, *27*, 283−287.
(18) Vogel, E. A. *Adv. Colloid Interface Sci.* **1998**, *74*, 69−117.
(19) Lee, J. H.; Lee, H. B.; Andrade, J. D. *Prog. Polym. Sci.* **1995**, *20*, 1043−1079.
(20) (a) Prime, K. L.; Whitesides, G. M. *Science* **1991**, *252*, 1164−1167. (b) Prime, K. L.; Whitesides, G. M. *J. Am. Chem. Soc.* **1993**, *115*, 10714−10721. (c) Sigal, G. B.; Mrksich, M.; Whitesides, G. M. *J. Am. Chem. Soc.* **1998**, *120*, 3464−3473.
(21) (a) Malmsten, M.; Emoto, K.; Van, Alstine, J. M. *J. Colloid Interface Sci.* **1998**, *202*, 507−517. (b) Vadgama, P. *Annu. Rep. Prog. Chem., Sect. C: Phys. Chem.* **2005**, *101*, 14−52. (c) Tokumitsu, S.; Liebich, A.; Herrwerth, S.; Eck, W.; Himmelhaus, M.; Grunze, M. *Langmuir* **2002**, *18*, 8862−8870. (d) Capadona, J. R.; Collard, D. M.; García, A. J. *Langmuir* **2003**, *19*, 1847−1852. (e) Snellings, G. M. B. F.; Vansteenkiste, S. O.; Corneillie, S. I.; Davies, M. C.; Schacht, E. H. *Adv. Mater.* **2000**, *12*, 1959−1962.
(22) Harris, J. M. *Poly(ethylene glycol) Chemistry: Biotechnical and Biomedical Applications*; Plenum: New York, 1992.
(23) (a) Wang, R. Y.; Himmelhaus, M.; Fick, J.; Herrwerth, S.; Eck, W.; Grunze, M. *J. Chem. Phys.* **2005**, *122*, 164702.1−164702.6. (b) Wang, R. L. C.; Jürgen Kreuzer, H.; Grunze, M. *Phys. Chem. Chem. Phys.* **2000**, *2*, 3613−2622.
(24) Wang, R. L. C.; Kreuzer, H. J.; Grunze, M. *J. Phys. Chem. B* **1997**, *101*, 9767−9773.

surfaces at high density.[25] However, on Ag surfaces, PEG chains are much more densely packed, forcing the chains into an extended all *trans* conformation, preventing hydration, which in turn allows protein adsorption. At the other extreme, low densities of surface-bound PEG cannot create a uniform hydrated layer and will not prevent protein adsorption. Thus, controlling both the density and conformation of presented PEG chains is important in creating a coating that repels proteins. Covalent grafting of PEG, including the use of PEG-functionalized SAMs,[26] has been extensively utilized by a number of groups to produce surfaces with different densities of PEG.[27] Additionally, a range of processing steps has allowed grafting on surfaces that do not normally have the proper chemical functionality for covalent grafting.[26b,27a,28,29] An alternative approach of surface attachment uses physisorbed assemblies, including Langmuir–Blodgett films,[15,30] that present PEG from the surface.[31] In particular, one of us has used surfactant-like polymers to assemble on a surface and display functional groups.[32] While initial studies were carried out on HOPG, this approach was found to work on a variety of hydrophobic surfaces, allowing presentation of biofunctional groups that in turn can influence biological processes. However, even though high densities of functional groups have been obtained, precisely controlling the surface density and lateral placement of functional groups has remained a challenge. A tunable, supramolecular surface scaffold that presents PEG chains could more precisely control surface density and could allow more accurate mechanistic studies of protein adsorption on PEG surfaces to be conducted.

Results and Discussion

In order to create self-assembling molecular scaffolds, which are able to present functional groups from a surface, a better understanding of what role the different structural components within these monomers play in the surface self-assembly is required. In a previous communication,[13] we showed that ditopic

Scheme 1. Synthesis of **G1$_n$G** (n = 8, 10, 12, 18) and Deprotection to Generate **G2$_n$G** (n = 12, 18)^a
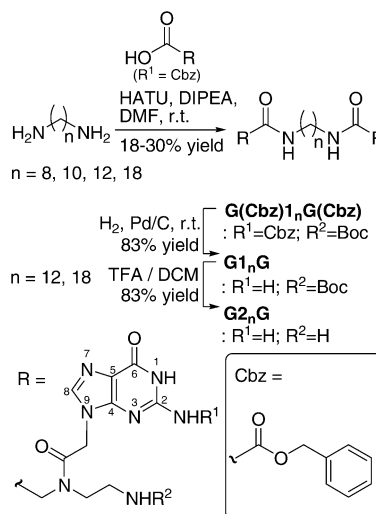
^{a} These ditopic monomers have a $-(CH_2)_n-$ hydrocarbon core flanked by guanine end groups (R).

monomers, consisting of either C_{12} or C_{18} linear alkyl chains with guanine peptide nucleic acid (PNA) end groups could result in the formation molecular-sized bands on HOPG when adsorbed from a water/DMSO solution. By building on this preliminary work and with the goal of further understanding the nature and mechanism of the surface self-assembly processes, we designed and synthesized a series of simple model compounds (**G1$_n$G**). These model monomers comprise three components, (1) a hydrocarbon core with n (= 8, 10, 12, 18) methylene groups, to enhance adsorption onto a hydrophobic surface in the presence of an aqueous medium, (2) the guanine end groups, to facilitate adsorbate–adsorbate interactions through hydrogen bonding, and (3) peptide nucleic acid (PNA)[33] chains primarily used to link the hydrocarbon cores and the guanine moieties. These monomers were prepared by reacting commercially available benzyl carbamate (Cbz)-protected guanine–PNA groups with 1,8-diaminooctane (n = 8), 1,10-diaminodecane (n = 10), 1,12-diaminododecane (n = 12), or 1,18-diaminooctadecane (n = 18) using standard peptide coupling conditions to produce **G(Cbz)1$_n$G(Cbz)** (Scheme 1). The guanine moieties were then deprotected using H_2 gas with a Pd/C catalyst to produce **G1$_n$G** (15–25% overall yield). The structures for the materials were confirmed by NMR and MALDI-MS.

As the monomers were not water soluble, surface self-assembly experiments were carried out by introducing a small amount (ca. 5 μL) of a DMSO monomer solution (0.94–5.4 mM, 1–5 μg/mL) into a water droplet (ca. 20 μL) on HOPG. A 1 mL fluid cell was then placed on top of the HOPG, and images of the surface were captured using a fluid tapping AFM setup at ambient temperature. All the monomers adsorbed on the surface within seconds, as measured by a change in surface roughness relative to bare HOPG, but no order was observed. However, upon addition of enough water to fill the 1 mL cell (yielding an overall concentration of the monomers of about 4.7–27 nM and diluting the DMSO to ca. 0.5%), two sets of linear band patterns were observed in all samples: a molecular-sized set of bands with widths <5 nm and a larger set of bands

(25) (a) Harder, P.; Grunze, M.; Dahint, R.; Whitesides, G. M.; Laibinis, P. E. *J. Phys. Chem. B* **1998**, *102*, 426–436. (b) Feldman, K.; Hähner, G.; Spencer, N. D.; Harder, P.; Grunze, M. *J. Am. Chem. Soc.* **1999**, *121*, 10134–10141.

(26) (a) Credo, G. M.; Boal, A. K.; Das, K.; Galow, T. H.; Rotello, V. M.; Feldheim, D. L.; Gorman, C. B. *J. Am. Chem. Soc.* **2002**, *124*, 9036–9037. (b) Zhu, X.-Y.; Jun, Y.; Staarup, D. R.; Major, R. C.; Danielson, S.; Boiadjiev, V.; Gladfelter, W. L.; Bunker, B. C.; Guo, A. *Langmuir* **2001**, *17*, 7798–7803. (c) Sanyal, A.; Norsten, T. B.; Uzun, O.; Rotello, V. M. *Langmuir* **2004**, *20*, 5958–5964. (d) Zou, S.; Zhang, Z.; Förch, R.; Knoll, W.; Schönherr, H.; Vancso, G. J. *Langmuir* **2003**, *19*, 8618–8621. (e) Garcia-Lopez, J. J.; Zapotoczny, S.; Timmerman, P.; van Veggel, F. C. J. M.; Vancso, G. J.; Crego-Calama, M.; Reinhoudt, D. N. *Chem. Commun.* **2003**, 352–353.

(27) (a) Jo, S.; Park, K. *Biomaterials* **2000**, *21*, 605–616. (b) Papra, A.; Gadegaard, N.; Larsen, N. B. *Langmuir* **2001**, *17*, 1457–1460. (c) Yang, Z.; Galloway, J. A.; Yu, H. *Langmuir* **1999**, *15*, 8405–8411.

(28) Chen, H.; Zhang, Z.; Chen, Y.; Brook, M. A.; Sheardown, H. *Biomaterials* **2005**, *26*, 2391–2399.

(29) Ghosh, P.; Amirpour, M. L.; Lackowski, W. M.; Pishko, M. V.; Crooks, R. M. *Angew. Chem., Int. Ed.* **1999**, *38*, 1592–1595.

(30) (a) Ulman, A. *An Introduction to Ultrathin Organic Films from Langmuir-Blodgett to Self-Assembly*; Academic Press: San Diego, 1991. (b) Peng, J. B.; Barnes, G. T.; Gentle, I. R. *Adv. Colloid Interface Sci.* **2001**, *91*, 163–219.

(31) (a) Vacheethasanee, K.; Wang, S.; Qiu, Y.; Marchant, R. E. *J. Biomater. Sci. Polym. Ed.* **2004**, *15*, 95–110. (b) Tae, G.; Lammertink, R. G. H.; Kornfield, J. A.; Hubbell, J. A. *Adv. Mater.* **2003**, *15*, 66–69. (c) Kim, K.; Kim, C.; Byun, Y. *J. Biomed. Mater. Res.* **2000**, *52*, 836–840.

(32) (a) Holland, N. B.; Qiu, Y.; Ruegsegger, M.; Marchant, R. E. *Nature* **1998**, *392*, 799–801. (b) Ruegsegger, M. A.; Marchant, R. E. *J. Biomed. Mater. Res.* **2001**, *56*, 159–167. (c) Sagnella, S.; Anderson, E.; Sanabria, N.; Marchant, R. E.; Kottke-Marchant, K. *Tissue Engin.* **2005**, *11*, 226–236. (d) Larsen, C. C.; Kligman, F.; Kottke-Marchant, K.; Marchant, R. E. *Biomaterials* **2006**, *27*, 4846–4855. (e) Larsen, C. C.; Kligman, F.; Tang, C.; Kottke-Marchant, K.; Marchant, R. E. *Biomaterials* **2007**, *28*, 3537–3548.

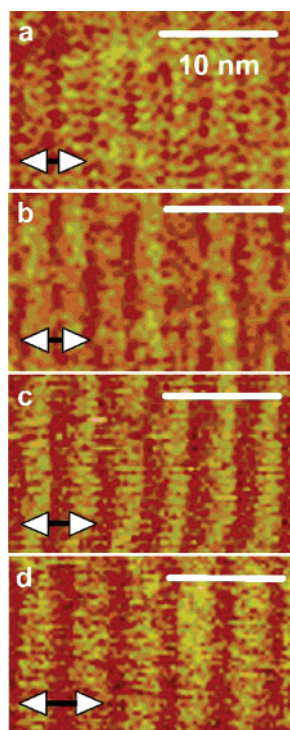(33) Nielson, P. E. *Acc. Chem. Res.* **1999**, *32*, 624–630.

Figure 2. AFM phase images of (a) **G1$_8$G**, (b) **G1$_{10}$G**, (c) **G1$_{12}$G**, and (d) **G1$_{18}$G** molecular-sized bands on HOPG. Band spacing increases with increasing length of the hydrocarbon core.

Table 1. Summary of Observed and Modeled Results[a] from Single Monomer Studies

M	L (nm)	W_{obs} (nm)	W_{mod} (nm)
G1$_8$G	3.6	3.2 ± 0.1	3.4
G1$_{10}$G	3.9	3.5 ± 0.1	3.6
G1$_{12}$G	4.2	3.8 ± 0.1	3.8
G1$_{18}$G	4.8	4.8 ± 0.1	4.9
G2$_{12}$G	4.2	3.8 ± 0.2	3.8
G2$_{18}$G	4.8	4.5 ± 0.2	4.4
G3G	3.4	2.5 ± 0.1	2.5
		3.4 ± 0.1	3.4
G4G	4.4	3.8 ± 0.1	3.8

[a] Summary of end-to-end length (L) of monomers (M) in extended conformation (from molecular modeling), width of observed bands (W_{obs}) on HOPG from AFM phase images, and width of modeled bands (W_{mod}) in energy-minimized models.

with widths between 5 and 7 nm. The widths of the molecular-sized bands were dependent on the length of the hydrocarbon core in the assembling monomer. For example, **G1$_8$G**, **G1$_{10}$G**, **G1$_{12}$G**, and **G1$_{18}$G** had widths of 3.2 ± 0.1, 3.5 ± 0.1, 3.8 ± 0.1, and 4.8 ± 0.1 nm, respectively (Figure 2a–d, Table 1) as measured by power spectrum and cross-sectional analyses. Thus, the band widths of molecular-sized bands in the **G1$_n$G** assemblies can be simply tuned by changing the hydrocarbon length (n). On the other hand, the widths of the larger bands, which showed more variability (multiple widths between 5 and 7 nm are observed) within the same monomer experiment, showed no correlation with the size of the monomers. These larger assemblies form distinctly separate domains from assemblies composed of molecular-sized bands. To date we have not been able to identify the exact nature of these "larger" bands, although it is possible that they consist either of multilayers or hemimicellar assemblies.[34]

Images captured at larger scan sizes (>500 nm) showed that there were many linear band assemblies that spanned areas as
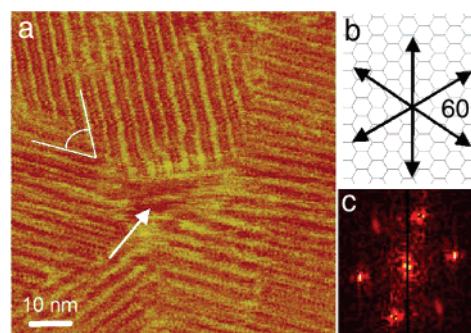

Figure 3. (a) AFM phase image of **G1$_{12}$G** domains offset by 60° (angular measurement). Domain boundary defects exist where the different domains meet (arrow). The angular offset of the domains suggests epitaxial assembly along the (b) symmetric axes of the HOPG lattice. (c) 2D Fourier transform of AFM image showing epitaxial organization of domains.

small as 50 nm and as large as 2 μm (see Supporting Information). The linear bands in each domain were offset from each other by a multiple of 60°, suggesting epitaxial alignment of the molecules along the three axes of symmetry in the HOPG lattice (Figure 3). Between the majority of the domains, amorphous boundary regions (arrow in Figure 3a) are observed where the linear bands do not connect and the assembly cannot continue growing because of interference from adjacent domains. Additionally, the presence of multiple domains suggests that there are multiple sites of nucleation.

The focus of this current research is the creation of tunable self-assembling molecular scaffolds. Thus, the fact that tailoring the molecular structure allowed the width of molecular-sized bands to be tuned suggests that these assemblies, rather than the larger band assemblies, are potential candidates for molecular scaffolds. Interestingly, as the length of the hydrocarbon core in the monomers increased, the prevalence of the larger bands in the surface assemblies decreased. For instance, **G1$_8$G** and **G1$_{10}$G** assemblies were composed mostly of larger bands with very few domains of molecular-sized bands. However, molecular-sized bands were found to occupy a significantly larger proportion of the surface in **G1$_{12}$G** coatings and were even more ubiquitous in **G1$_{18}$G** coatings. As a result, the latter two monomers are better suited to create tunable scaffold coatings, and thus, these monomers became the major focus of this research.

On the basis of the molecular design of **G1$_n$G**, it was expected that hydrogen bonding, most likely through guanine–guanine interactions, would play a role in the surface assembly. Thus, the surface assembly of two controls, a monomer with reduced hydrogen-bonding capability (**G(Cbz)1$_{12}$G(Cbz)**) and 1,12-diaminododecane, were characterized. **G(Cbz)1$_{12}$G(Cbz)** is a precursor to **G1$_{12}$G** and is protected at the guanine C(2) exo-amino site by a Cbz group, resulting in greatly reduced Watson–Crick hydrogen-bond interactions. Fluid tapping mode imaging of HOPG coated with **G(Cbz)1$_{12}$G(Cbz)** revealed only the large bands (5–7 nm widths) and amorphous domain boundary regions, with no sign of the molecular-sized bands. This suggests that blocking the Watson–Crick face of the guanine greatly reduces the tendency of **G(Cbz)1$_{12}$G(Cbz)** to self-assemble into

(34) (a) Wanless, E. J.; Davey, T. W.; Ducker, W. A. *Langmuir.* **1997**, *13*, 4223–4228. (b) Nishimura, S.; Scales, P. J.; Biggs, S. R.; Healy, T. W. *Colloid Surf. A.* **1995**, *103*, 289–298. (c) Manne, S.; Cleveland, J. P.; Gaub, H. E.; Stucky, G. D.; Hansma, P. K. *Langmuir.* **1994**, *10*, 4409–4413. (d) Fuhrhop, J. H.; Wang, T. *Chem. Rev.* **2004**, *104*, 2901–2937.

stable molecular-sized bands. The second control, 1,12-diami-nododecane, adsorbed on the HOPG surface; however, it also did not form the molecular-sized bands, under the conditions described previously, suggesting the importance of having guanine end groups for the desired tunable band spacings observed in the **G1$_n$G** assemblies.

The above results suggest that the hydrogen-bonding ability of the guanine is important to the formation of the molecular-sized bands. The question then becomes how the guanine is self-assembling on the surface. From the literature it is known that guanine and its 9-substitued derivatives form linear tapelike structures, in solution,[9,11,35] the solid state,[9,11,36] and on surfaces.[9,10,11,37] Two major guanine motifs have been identified/proposed. The first is a non-dipole guanine motif (Figure 4a), which has been observed in STM images of guanine monolayers[10a] on graphite and proposed in the crystal structures of some guanine derivatives.[38] This guanine motif forms centrosymmetric repeat units, centered between the two guanines (G1 and G2 in Figure 4a), along the hydrogen-bonded chain. As a result of this symmetry there is no net dipole in this motif. When the R group on N(9) is bulky or in the crystal structures of some guanine derivatives,[38] the guanine moieties can instead form a different guanine tape motif (Figure 4b), presumably, on account of the steric repulsions between adjacent R groups.[10b,11] In this case the motif is no longer centrosymmetric, and this results in a net dipole along the entire structure (arrow in Figure 4b). These two known guanine motifs became the starting point for molecular modeling studies with the goal of developing a better understanding of how the **G1$_n$G** molecules may be arranging within the molecular-sized bands.

Molecular modeling of all the **G1$_n$G** monomers, using the consistent valence forcefield (CVFF, class I forcefield) in DISCOVER, were carried out on a modeled graphene surface and in a simulated aqueous environment (distance-dependent dielectric $\epsilon_r = 80$). The first sets of modeling experiments were carried out on **G1$_{12}$G** using either of the two guanine motifs shown in a and b of Figure 4 (see Supporting Information). However, the resulting modeled assemblies suggested the formation of bands with widths of ca. 3.4 nm that did not match observed 3.8 nm bands measured by AFM. Thus, other possible guanine motifs were investigated. Interestingly, a double-stranded guanine tape motif (Figure 4c) was found that resulted in assemblies with modeled band widths that more correctly predicted the observed 3.8 nm bands (Figure 5a) and was of lower calculated energy than the models of either of the previously described motifs. This centrosymmetric double-stranded motif is composed of guanine dimers formed through the Watson–Crick faces of two guanine moieties. This dimeric
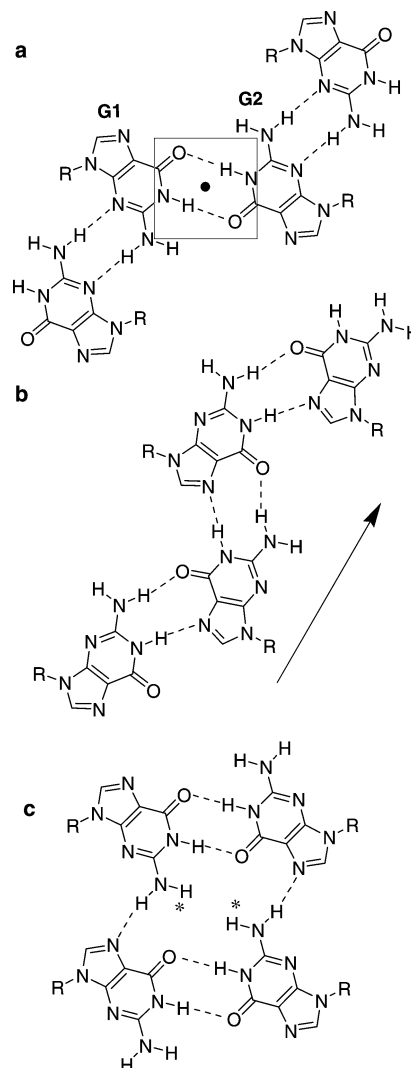
(35) (a) Gottarelli, G.; Masiero, S.; Mezzina, E.; Spada, G. P. *Helv. Chim. Acta* **1998**, *81*, 2078–2092. (b) Giorgi, T.; Grepioni, F.; Manet, I.; Mariani, P.; Masiero, S.; Mezzina, E.; Pieraccini, S.; Saturni, L.; Spada, G. P.; Gottarelli, G. *Chem. Eur. J.* **2002**, *8*, 2143–2152. (c) Yoshikawa, I.; Yanagi, S.; Yamaji, Y.; Araki, K. *Tetrahedron* **2007**, *63*, 7474–7481.
(36) (a) Forman, S. L.; Fettinger, J. C.; Pieraccini, S.; Gottarelli, G.; David, J. T. *J. Am. Chem. Soc.* **2000**, *122*, 4060–4067. (b) Thewalt, U.; Bugg, C. E.; Marsh, R. E. *Acta. Crystallogr.* **1971**, *B27*, 2358–2363. (c) Calzolari, A.; Di Felice, R.; Molinari, E.; Garbesi, A. *Physica E* **2002**, *13*, 1236–1239.
(37) (a) Srinivasan, R.; Murphy, J. C.; Fainchtein, R.; Patabiraman, N. *J. Electroanal. Chem. Interfacial Electrochem.* **1991**, *312*, 293–300. (b) Tao, N. J.; Shi, Z. *J. Phys. Chem.* **1994**, *98*, 1464–1471. (c) Otero, R.; Schöck, M.; Molina, L. M.; Lægsgaard, E.; Stensgaard, I.; Hammer, B.; Besenbacher, F. *Angew. Chem., Int. Ed.* **2005**, *44*, 2270–2275.
(38) (a) Thewalt, U.; Bugg, C. E.; Marsh, R. E. *Acta Crystallogr.* **1970**, *B26*, 1089–1101. (b) Thewalt, U.; Bugg, C. E.; Marsh, R. E. *Acta Crystallogr.* **1971**, *B27*, 2358–2363.
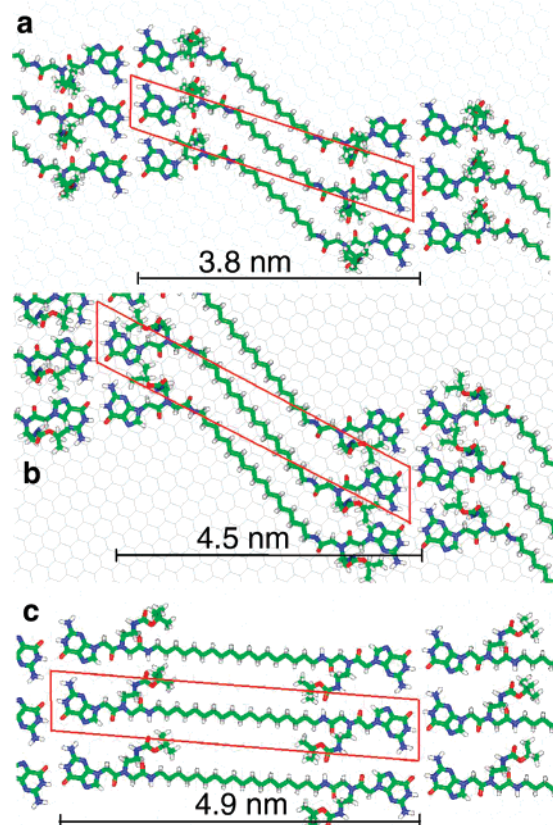
Figure 4. (a) Non-dipole guanine motif with centrosymmetric interactions (i.e., center of symmetry between G1 and G2 indicated by dot), (b) dipole tape motif with net dipole (arrow), and (c) dimer motif with C(2) exo-amino hydrogens (*) separated by 3 Å.

motif is extended into a tape through additional nucleobase hydrogen bonding through the exo-NH_2 and N(7) on the Hoogsteen face of adjacent guanine dimer moieties. While two of the exo-amino hydrogens (* in Figure 4c) are in close proximity, modeling indicates that these atoms are separated by 3 Å with no van der Waals overlap.

It is possible that the PNA-Boc groups within the **G1$_{12}$G** assemblies sterically hinder the formation of the guanine motif shown in Figure 4a. There are potentially a number of reasons why the double-stranded motif appears to be more energetically favored over the motif in Figure 4b. These include better packing efficiency on the surface, enhanced surface–absorbate interactions, and the lack of a dipole in the double-stranded guanine tape.

Models of the **G1$_8$G** and **G1$_{10}$G** assemblies using this double-stranded guanine motif also showed lower modeled energies than the models using the motifs in a and b of Figure 4. In addition, the models also predicted the banding patterns to be 3.4 and 3.6 nm, respectively, which match much better with the observed AFM patterns (3.2 and 3.5 ± 0.1 nm, respectively) than the patterns predicted by the models using the other two guanine motifs.

Figure 5. Energy-minimized molecular models of (a) $G1_{12}G$ in a close-packed arrangement, (b) $G1_{18}G$ in a close-packed arrangement, and (c) $G1_{18}G$ in an open hydrocarbon arrangement. Modeled band spacing (nm) and unit cell (box) for each proposed arrangement is also shown.

Figure 6. (a) Chemical structure of $G3G$. (b) AFM phase image of multiple domains of $G3G$ ("brighter" areas) forming molecular-sized bands with widths of 2.5 nm (arrows) and 3.4 nm (circle). Surface coverage is incomplete with surrounding "darker" regions having an amorphous phase.

In all of the previous models the hydrocarbons are close packed, presumably to maximize packing efficiencies. Interestingly, molecular modeling of $G1_{18}G$ assemblies with close-packed alkyl chains (Figure 5b) suggested a band spacing of 4.5 nm, which is significantly less than the observed 4.8 ± 0.1 nm by AFM. Further modeling studies found that a more open hydrocarbon arrangement (Figure 5c) not only yielded a better prediction (4.9 nm) of the observed band spacing but also was lower in energy than the close-packed structure. Models of $G1_8G$, $G1_{10}G$, and $G1_{12}G$ in the open alkyl arrangement, however, all had higher modeled energies than the models of their alkyl close-packed assemblies. Furthermore, the predicted band spacings from these open arrangements were much larger than the experimentally observed ones. Thus, there seems to be a change in the arrangement of hydrocarbons going from small hydrocarbons ($n = 8, 10, 12$) to the larger one ($n = 18$). The exact reason for this change in hydrocarbon arrangement is not known; although based on the model (Figure 5c), it appears that the Boc groups play an important role. In the open arrangement of $G1_{18}G$ the Boc group is adsorbed onto the graphite surface, and there appears to be hydrogen bonding between the amide N–H and carbamate C=O of adjacent molecules. In the more close-packed arrangement (Figure 5b) the Boc groups sit on top of the molecules, and there is no amide–carbamate hydrogen bonding.

Thus, to further investigate the influence of the PNA-Boc linker group on the surface self-assembly a number of different ditopic guanine monomer derivatives were studied. A first set of experiments were carried out on monomers in which the Boc
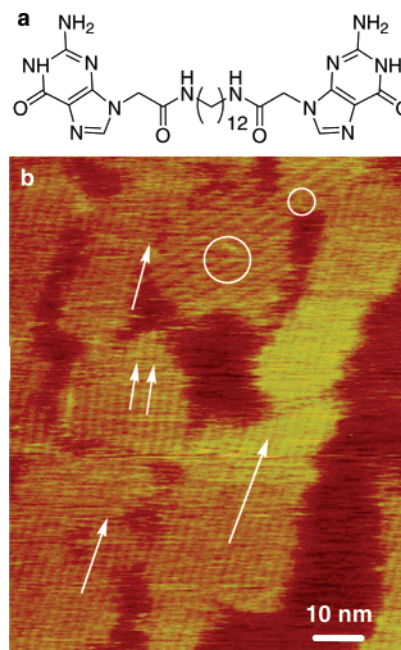
protecting groups had been removed. If, as suggested above, the Boc groups play a role in aiding the formation of the "open" conformation in $G1_{18}G$, then it would be expected that removing its Boc groups should result in a significant change in the band spacing. However, if $G1_{12}G$ is already in the "closed" conformation as modeling suggests, then removal of the Boc groups from this monomer would not significantly affect its assembly. Standard Boc deprotection chemistry (trifluoroacetic acid) was used to generate $G2_{12}G$ from $G1_{12}G$ and $G2_{18}G$ from $G1_{18}G$. The removal of the two hydrophobic Boc groups, not surprisingly, makes $G2_{12}G$ and $G2_{18}G$ more water soluble. As such, this has consequences for the surface assembly from aqueous environments. A higher monomer concentration ($11-17 \mu M$, in DMSO yielding an overall concentration of $55-85$ nM after addition of water) was needed before ordered assemblies on the surface could be observed. Additionally, the bands were less stable compared to $G1_nG$ monomer assemblies, making the $G2_nG$ assemblies more prone to disruption by the AFM probe. AFM experiments of $G2_{12}G$ on HOPG showed molecular-sized bands with 3.8 ± 0.2 nm repeats, the same widths observed in $G1_{12}G$ assemblies, indicating the Boc groups do not significantly alter the spacing of the molecular-sized bands in this system. Models confirm these findings, as there is no change in band spacing or monomer arrangement once the Boc groups are removed (see Supporting Information). On the other hand, when $G2_{18}G$ was assembled on HOPG, it was found to form band spacings of 4.5 ± 0.2 nm. Interestingly, this corresponds to a close-packed alkyl arrangement (see Supporting Information). This suggests that the Boc groups in $G1_{18}G$ play a role in aiding the assembly of the C_{18} hydrocarbon core into the open arrangement. Removal of the Boc groups did not seem to affect the assembly of larger bands ($5-7$ nm) as they were still observed.

To examine the effect that the PNA linker group has on the assembly of these systems $G3G$ (Figure 6a), which is simply a

ditopic guanine endcapped dodecane with no PNA linker groups, was designed and synthesized. These monomers were synthesized in 23% overall yield by reacting guanine(Cbz) acetic acid[39] with 1,12-diaminododecane, using standard peptide-coupling conditions, followed by hydrogenation. Like **G1**$_n$**G**, **G3G** assembled into epitaxially aligned molecular-sized bands; however, unlike **G1**$_n$**G**, different molecular-sized banding spacings, namely 2.5 ± 0.1 nm and 3.4 ± 0.1 nm, were observed within different domains in the same experiment (Figure 6b). It should be noted that, while some of the domains appear to have offsets that are at slightly different angles (offset by ∼5°) from normal epitaxial angles, this is most likely a consequence of disruption from the AFM tip due to repeated scanning, possibly suggesting that **G3G** domains are less stable than the **G1**$_n$**G** domains.

Molecular modeling was again used to help understand the arrangement of the molecules within these molecular-sized band assemblies. Assemblies of **G3G** were modeled using all three surface guanine motifs outlined in Figure 4 (see Supporting Information). A model using the guanine motif in Figure 4a had bands that matched the 2.5 nm band spacing, and a model using the double-stranded guanine motif (Figure 4c) had modeled band widths that matched the observed 3.4 nm band spacing with the latter having a lower energy. Not surprisingly, it is difficult to model two or more different guanine motifs within the same domain as the alignment of the molecules changes because of the nature of the different guanine–guanine interactions. Thus, it is not surprising that each domain of **G3G** has only a single bandwidth and is not composed of both 2.5 and 3.4 nm bands. These experiments suggest that the PNA linker in **G1**$_n$**G** hinders the formation of the guanine tape in Figure 4a, presumably on account of steric repulsions, thus only allowing the system to assemble through one guanine motif, namely the double-stranded assembly. This is an important consideration if regular repeatable banding structures are targeted for the surface scaffolds.

One of the strengths of our monomer scaffold design is, potentially, the ability to tune the assembly by combining differently sized monomers. For example, since our models predicted that both **G1**$_{12}$**G** and **G1**$_{18}$**G** formed the double-stranded guanine motif, the two different monomers would be expected to assembly together within the same assembly. However, modeling studies suggested structures that contained both **G1**$_{12}$**G** and **G1**$_{18}$**G** within one band are not favored because of the length mismatch (six methylene groups) of these monomers. Thus, the only way to ensure that both of the chain-end guanines are involved in hydrogen bonding is for the different monomers (**G1**$_{12}$**G** and **G1**$_{18}$**G**) to separate into different bands (Figure 7), resulting in a surface assembly which contains two differently sized banding patterns within the same domain. Since there is no hydrogen-bonding specificity between the different monomers, the order of bands is expected to be random. The relative surface concentration of two different monomer species was also investigated, as it is well-known that longer *n*-alkanes have a much larger surface–adsorbate interaction with graphite compared to shorter *n*-alkanes.[5] Therefore,
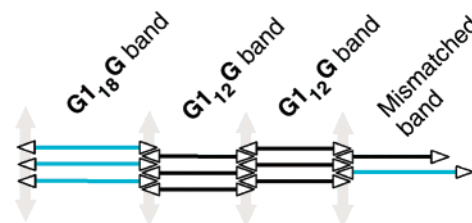
(39) (a) Dueholm, K. L.; Egholm, M.; Behrens, C.; Christensen, L.; Hansen, H. F.; Vulpius, T.; Petersen, K. H.; Berg, R. H.; Nielson, P. E.; Buchardt, O. *J. Org. Chem.* **1994**, *59*, 5767–5773. (b) Thomson, S. A.; Josey, J. A.; Cadilla, R.; Gaul, M. D.; Hassman, C. F.; Luzzio, M. J.; Pipe, A. J.; Reed, K. L.; Ricca, D. J.; Wiethe, R. W.; Noble, S. A. *Tetrahedron* **1995**, *51*, 6179–6194.
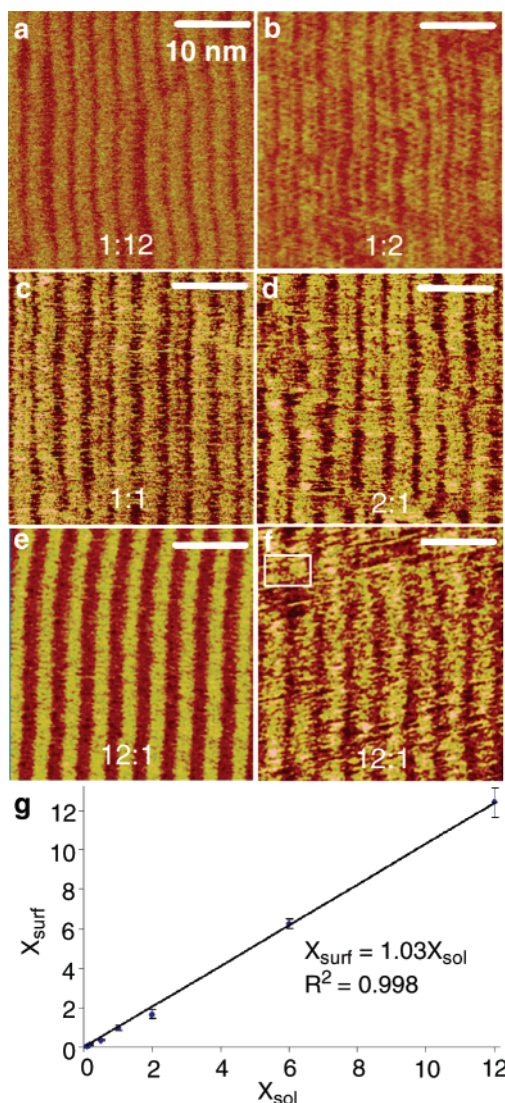
Figure 7. Concept of **G1**$_{18}$**G** (light) and **G1**$_{12}$**G** (dark) combined assembly into molecular-sized bands. Molecules will favor phase separation on account of mismatched guanines when they assemble in the same band.

it was expected that **G1**$_{18}$**G** would have a higher surface concentration relative to **G1**$_{12}$**G** when the two sets of monomers were deposited onto HOPG from a mixture of the two in solution.

Using procedures similar to those described previously, premixed monomer solutions with varying molar ratios of **G1**$_{12}$**G** and **G1**$_{18}$**G** were used in surface-assembly experiments. Four representative phase images (a–d of Figure 8) qualitatively show the change in surface assembly that results as the molar ratio of the monomers **G1**$_{18}$**G**/**G1**$_{12}$**G** is changed from 1:12 to 2:1. Nanophase separation of the two monomers is indeed observed in all these cases, resulting in two different molecular-sized band widths (3.9 ± 0.1 and 4.5 ± 0.1 nm most likely correspond to bands formed by **G1**$_{12}$**G** and **G1**$_{18}$**G**, respectively) that occur within the same domain. When compared to the observed characteristic single monomer assemblies (Figure 2c,d), the bandwidth of **G1**$_{12}$**G** in the combined assembly is within experimental error of the observed 3.9 nm, while the assigned 4.5 nm is 0.3 nm shorter than the open arrangement (Figure 5c) **G1**$_{18}$**G** band spacing. However, the 4.5 nm band spacing does match with the **G1**$_{18}$**G** assembly that has a close-packed hydrocarbon arrangement (Figure 5b). This suggests that, in combined assemblies of **G1**$_{12}$**G** and **G1**$_{18}$**G**, not only does the difference in size of the hydrocarbon cores result in nanophase separation of the molecules, but the arrangement of **G1**$_{12}$**G** also seems to influence the packing arrangement of the hydrocarbons in **G1**$_{18}$**G**. This then suggests a possible explanation for the 4.5 nm **G1**$_{18}$**G** bands. The presence of **G1**$_{12}$**G** molecules, which adopt a close-packed hydrocarbon arrangement, induce the **G1**$_{18}$**G** to adopt a similar close-packing structure that more closely resembles the structural and geometric requirements of the smaller assembly.

This leads to an interesting question, namely what happens to the assemblies when a large excess of one of the monomers is present? For example, Figure 9 shows a larger-area AFM image of the assembly in which a small amount of **G1**$_{18}$**G** is assembled with a large excess of **G1**$_{12}$**G** (ratio 1:12). In this case regions of wider banding patterns (4.5 nm) are observed within a smaller banding pattern (3.9 nm) matrix. This suggests that, as there is not enough **G1**$_{18}$**G** to form a complete single band, the **G1**$_{18}$**G** phase segregates within a **G1**$_{12}$**G** band, presumably to minimize the energy penalties required to fit the larger monomer into the smaller banding assembly. These are regions of nanophase-separated **G1**$_{18}$**G** spanning up to 50 nm, which from the modeled distances corresponds to a band containing ca. 63 molecules.

At the other extreme, mixtures of the two monomers with ratios skewed toward **G1**$_{18}$**G**, such as the 12:1 experiments (Figure 8e,f), result in the self-assembly of molecular-sized bands of 4.8 nm. This is consistent with the lower concentration

Figure 8. AFM phase images of two-monomer $G1_{18}G/G1_{12}G$ assemblies with solution molar ratios (a) 1:12, (b) 1:2, (c) 1:1, (d) 2:1, and (e,f) 12:1. Surface concentration of monomer bands matches the solution concentration. (e) $G1_{18}G$ bands with minimal $G1_{12}G$ produce bands of 4.8 nm. (f) $G1_{12}G$ (box) introduces defects into the $G1_{18}G$ assembly. (g) The ratio of surface mole fraction of $G1_{18}G$/surface mole fraction of $G1_{12}G$ (X_{surf}) vs the ratio of solution mole fraction of $G1_{18}G$/solution mole fraction of $G1_{12}G$ (X_{sol}) is plotted and shows a Langmuir-like correlation with a slope of 1.0.

Figure 9. AFM phase image of 1:12 $G1_{18}G/G1_{12}G$ surface assembly on HOPG. Nanophase-separated regions of $G1_{18}G$ are up to 50 nm. Bands with both monomers produce band defects (box). There is also a type of boundary domain defect (oval).

Figure 10. AFM phase images of $G1_{18}G$ coating captured at 50 °C showing presence of linear band assemblies. (a) Coating assembled at room temperature and then heated to 50 °C and (b) assembly created at 50 °C.

of $G1_{12}G$ not having as much of an influence on the $G1_{18}G$ assembly. In regions where the $G1_{12}G$ appears to be present (box in Figure 8f), more disorder is observed than in regions of the assembly that only seem to contain $G1_{18}G$ (Figure 8e).

Quantitatively, the surface coverage of each monomer within the assemblies of different monomer ratios was calculated and plotted. Interestingly, there is a linear trend with a slope of 1.0 that correlates the ratio of the solution mole fractions to the ratio of the surface mole fractions of the two monomers (Figure 8g) which suggests a Langmuir-like correlation.[40] Even though each methylene group that is commensurate with the HOPG lattice generates 6.28 kJ/mol of free energy,[5,41] there was no observed preference for the surface adsorption of $G1_{18}G$ over $G1_{12}G$.[13] As both monomers have two guanine PNA moieties,

(40) Masel, R. I. *Principles of Adsorption and Reaction on Solid Surfaces*; John Wiley & Sons, Inc.: New York 1996; pp 235−254.
(41) Findenegg, G. H.; Liphard, M. *Carbon* **1987**, *25*, 119−128.
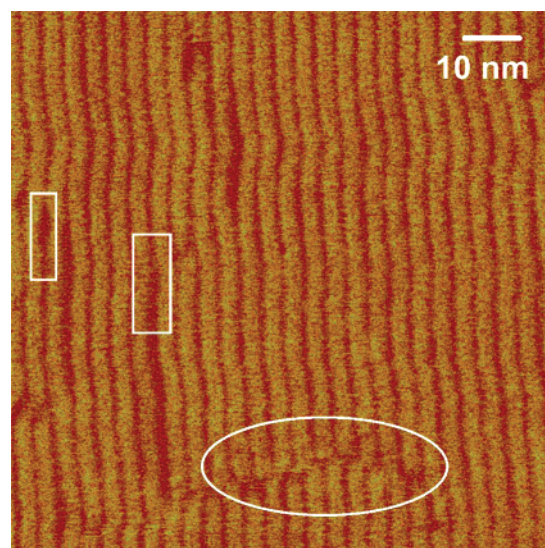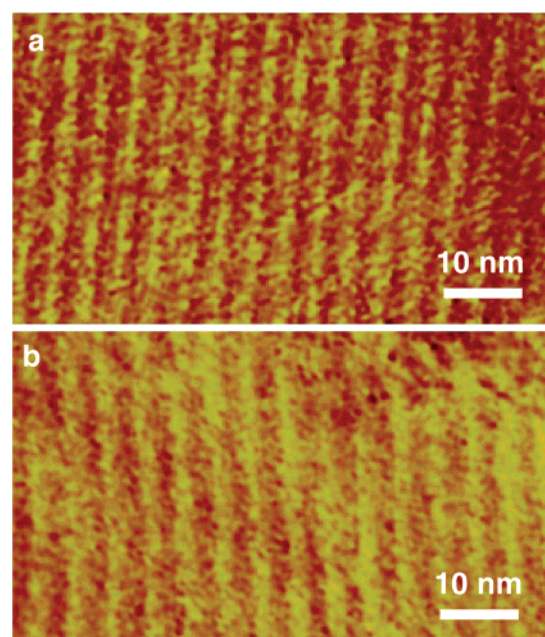
this suggests that the guanine PNA−HOPG and the guanine− guanine interactions are playing a significant role in the assembly.

All studies discussed to date were carried out at 28 °C. However, in order for these assemblies to be utilized in bioenvironments, they have to be stable at physiological temperatures. Thus, to probe the thermal stability of these assemblies in more detail, imaging studies of the $G1_{18}G$ coatings were carried out at temperatures (50 °C) much higher than would be required under physiological conditions. Linear band patterns were observed with coatings that were assembled at room temperature and imaged at 50 °C, an indication that these nanoassemblies are stable at this temperature (Figure 10a). In addition, studies were carried out to see if $G1_{18}G$ would

Scheme 2. Synthesis of **G4G**
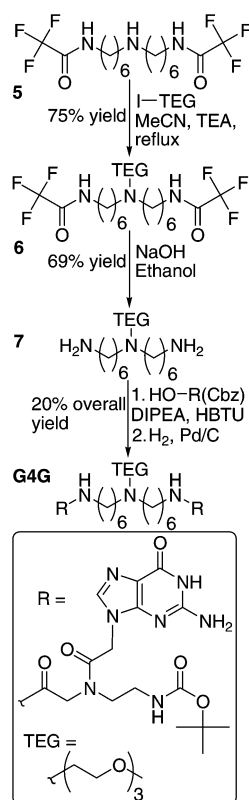
assemble at 50 °C. Thus, the HOPG surface with a water droplet on it was heated to 50 °C; this was followed by addition of the DMSO monomer solution to the water droplet before water (at 50 °C) was used to fill the fluid cell. Linear bands were again observed (Figure 10b), indicating that the intermolecular interactions that favor linear band assemblies are strong enough to both nucleate and assemble at 50 °C.

With the goal of using these assemblies to create oligo-(ethylene glycol)-covered surfaces, **G4G**, a monomer structurally similar to **G1₁₂G** with a triethylene glycol monomethyl ether (TEG) side chain was designed. The short-chain TEG was chosen to demonstrate the concept of the scaffold coating in part for ease of synthesis. In our proof-of-concept design, TEG is anchored from a tertiary amine that is located at the center of the hydrocarbon core that is flanked by two guanine PNA-Boc groups. The synthesis of **G4G** is outlined in Scheme 2. Iodo-TEG (see Supporting Information) was reacted with the protected bis(hexamethylene) triamine[42] (**5**) to yield **6**. After deprotection the resulting diamine (**7**) was converted into **G4G**, in 10% overall unoptimized yield from **5**, using procedures similar to those used to access the **G1ₙG** monomers.

The assembling ability of **G4G** was investigated using the procedures previously described; however, on account of the increased water solubility of **G4G**, higher concentrations (8–13 mM in DMSO) of the monomer were used. AFM fluid tapping mode images showed that **G4G** adsorbed immediately on HOPG as measured by a change in surface roughness. After diluting the DMSO with water, it took several minutes to an hour before linear bands were observed. Comparatively, **G1ₙG** band assemblies were observed almost immediately after dilution of DMSO with water. This may have to do with the greater
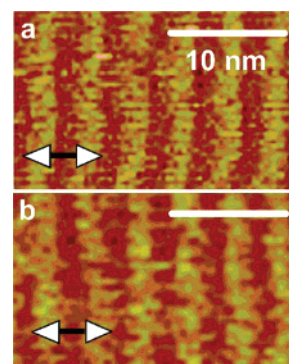
(42) Curphey, T. J. *J. Org. Chem.* **1979**, *44*, 2805–2807.

Figure 11. Comparison of the AFM phase images of (a) **G1₁₂G,** forming 3.8 nm bands, and (b) **G4G**, forming 3.8 nm bands. The 3.8 nm widths of both these assemblies suggests the molecules in both assemblies are arranging similarly.

water solubility of **G4G** or perhaps that the tertiary amine, which is presumably protonated at neutral pH, reduces the stability of the surface–adsorbate interactions. After a few hours, however, both epitaxial molecular-sized and larger bands were observed. The molecular-sized bands had widths of 3.8 ± 0.1 nm and are similar in width to the molecular-sized bands observed with **G1₁₂G** (Figure 11a,b). As is observed in the **G1₁₂G** case, the majority of the bands on the **G4G**-coated surface are the molecular-sized ones.

From the studies mentioned above (e.g., Figures 2, 8, and 9), it is believed that the dark bands in the AFM phase images correspond to the hydrocarbon segments and the lighter bands correspond to the PNA-Boc–nucleobase segments. Thus, it was expected that the TEG side group should be presented in the center of the darker band in the images. However, no sign of the TEG could be distinguished on AFM scans. This is possibly a consequence of the TEG being too small and flexible relative to any other part of the coating, thus hindering detection by the AFM tip.

Molecular modeling of **G4G** (Figure 12b) using a double-stranded motif and a close-packed arrangement similar to **G1₁₂G** shows modeled bands of 3.9 nm that match the observed band spacing. However, by adding an attachment point (the tertiary nitrogen) for the TEG, the number of core atoms between guanine PNA moieties changes from being even in **G1₁₂G** to being odd in **G4G**. As a result, the molecules close pack in a slightly different arrangement compared to **G1₁₂G** (Figure 12a,b). In this case, a pseudo-centrosymmetric assembly is predicted for the **G4G**, in which adjacent double-stranded guanine motifs run antiparallel with respect to each other, whereas in **G1₁₂G** they run parallel. Indeed, there have been many other reports of assemblies of small molecules that produce different packing arrangements for even and odd core atom parities.[7b,d,43] Modeling also suggests that the TEG groups are not large enough to completely cover the hydrophobic scaffold coating. Calculations from the models suggest a density of 0.32 TEG groups/nm².

If **G4G** has assembled on the surface as indicated by the models, then the HOPG has TEG groups supramolecularly grafted on to it. Thus, if the assembly is stable under biologically relevant conditions, this TEG coating of the HOPG should impart some effect on protein adhesion to the surface. However,

(43) Fang, H.; Giancarlo, L. C.; Flynn, G. W. *J. Phys. Chem. B* **1998**, *102*, 7421–7424.
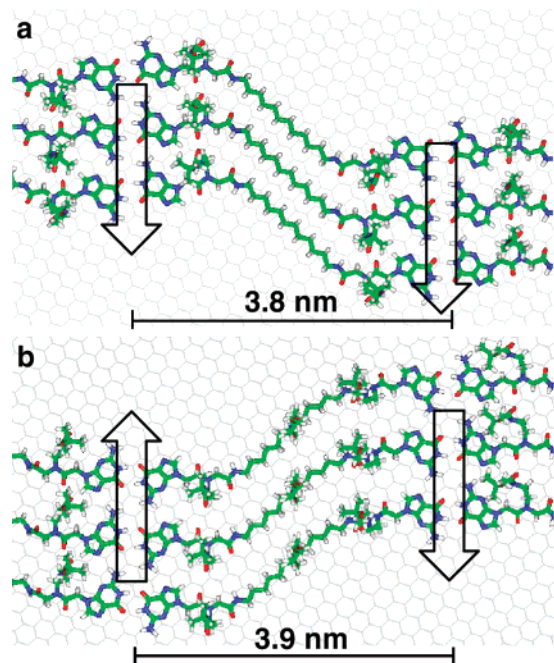
Figure 12. Energy-minimized molecular models of (a) **G1₁₂G**, and (b) **G4G** with modeled bands that match the observed band spacings. Change in number of core atoms changes packing arrangement of molecules so that adjacent guanine motifs run parallel in (a) and antiparallel in (b).

as mentioned before, the models suggest the TEG units do not completely cover the hydrophobic surface; thus, close to complete prevention of protein adhesion is not expected. Nonetheless, if this material shows any effect in hindering platelet adhesion, then derivatives which present an increased density of functional units, either by using higher-molecular weight PEG side chains or dendritic carbohydrate side chains,[44] could result in more dramatic effects being observed. Thus, initial studies to probe the biological effect of the current assembly were performed using static platelet adhesion. Platelets act indirectly as a marker for plasma protein adsorption and are a critical step in surface-induced thrombosis. Thus, four surfaces, bare HOPG, **G1₁₂G**-coated HOPG, **G4G**-coated HOPG, and **6**-coated HOPG, were prepared at room temperature and incubated with platelet-rich plasma (PRP). The samples were then fixed with paraformaldehyde, tagged with fluorescein isothiocyanate (FITC)-labeled anti-CD41a, which binds to the active site of the α subunit (GPIIb) of the GPIIb/IIIa platelet receptor, and mounted on slides. Between each step, the surfaces were washed three times with phosphate buffered saline (PBS) in order to remove any nonadherent platelets. Figure 13a−e shows representative epifluorescence optical microscopy images (400×) of platelets adhering from the PRP solution to (a) bare HOPG, (b) **G1₁₂G**-coated HOPG, (c) **G4G**-coated HOPG, and (d,e) **6**-coated HOPG. The percent surface coverage of the platelets was calculated using a threshold analysis. Static platelet adhesion on both the bare HOPG and the **G1₁₂G** coating were statistically equivalent with $34.6 \pm 5.6\%$, $37.6 \pm 6.7\%$ surface platelet coverage, respectively (Figure 13f). These coatings are both hydrophobic, and adhesion of a relatively large quantity of platelets was expected. However, surface platelet coverage on the **G4G** coating was $20.8 \pm 2.6\%$ which is statistically significant compared to either the bare HOPG ($p = 0.014$) or
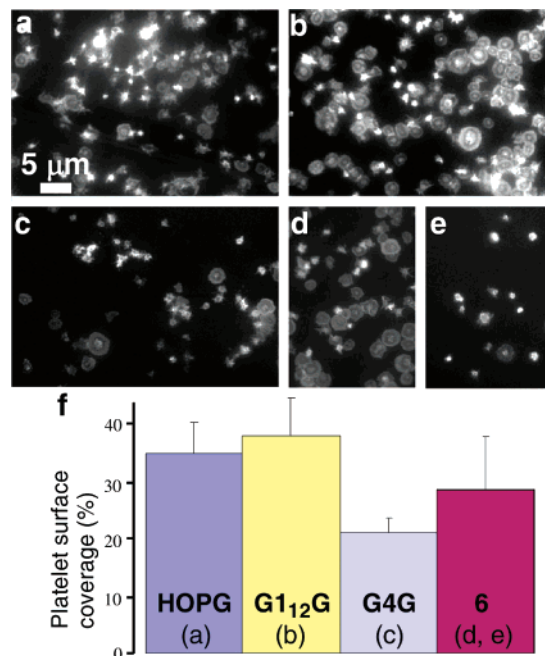
(44) Zhu, J.; Marchant, R. E. *Biomacromolecules* **2006**, *7*, 1036−1041.

Figure 13. Epifluoresence optical microscopy (400 ×) images showing static platelet adhesion on (a) bare HOPG, (b) **G1₁₂G**-coated HOPG, (c) **G4G**-coated HOPG, (d,e) **6**-coated HOPG. (f) Platelet surface coverage (%) vs surfaces ($n = 5$) demonstrating reduction in static platelet adhesion to $20.8 \pm 2.6\%$ on **G4G** coating relative to bare HOPG ($p = 0.014$) and the **G1₁₂G** coating. ($n = 5$, $p = 0.007$). **6**-coated HOPG had a large standard deviation due to regions that adhere platelets (d) similar to bare HOPG and (e) similar to **G4G**-coated HOPG.

the **G1₁₂G** coating ($p = 0.007$). The reduction in static platelet adhesion on **G4G** is consistent with the TEG side chain creating hydrated patches that repel plasma proteins and platelets. On all three surfaces, different morphologies of adherent platelets were observed, which likely represent different stages of platelet activation.

To understand the effect that the supramolecular network has in creating a uniform coating of TEG, surface studies of **6**, a synthetic precursor of **G4G** which does not have guanine−PNA end groups, were compared with **G4G**. **6** adsorbed onto HOPG, but no band assemblies were observed, and the adsorbed material was not stable to AFM fluid tapping mode imaging (see Supporting Information), suggesting that the extensive hydrogen-bonding mediated by the guanine−PNA units plays an important role in stabilizing **G4G** assemblies on HOPG. Static platelet adhesion studies on **6**-coated HOPG showed an average platelet coverage over the sample of $28.4 \pm 9.2\%$ (Figure 13f). The large standard deviation comes from the heterogeneous platelet coverage in this systems, some regions had platelet coverage similar to bare HOPG (Figure 13a) while other regions had platelet coverage closer to **G4G** surfaces (Figure 13c). These platelet adhesion results suggest that the guanine−PNA units in the **G4G** coatings help to present TEG side chains more uniformly. Thus, while it seems that the adsorption of TEG monomers on HOPG can influence platelet adhesion, studies with this control compound suggest that, with guanine−PNA end groups a supramolecular network is important to create a more uniform coating.

Conclusions

In these studies, tunable surface assemblies have been created using low-molecular weight ditopic monomers on a HOPG

surface. The assemblies are composed of bands with widths that can be systematically varied by simply changing the length of the core hydrocarbon unit. Furthermore, this concept has been extended into using these assemblies as scaffolds to supramolecularly graft groups (in this case TEG) onto HOPG. These grafted assemblies have been shown to be stable at biologically relevant temperatures and have even shown the ability to influence biological processes, namely static platelet adhesion. This concept of using the surface assemblies as scaffolds is potentially a very versatile one in which a wide range of biologically active (or other functionalities) can be envisaged, opening the door to systematic, facile functionalization of a surface using a simple dip-coating process.

JA0775927